for 30 min at room temperature (RT) to eliminate endogenous peroxidase activity. After incubation with 5% normal goat serum (NGS) in PBST for 1 h at RT, the sections were incubated with primary antibody (rabbit anti-β-gal, 5′ → 3′, Boulder, CO, 1:500; rabbit anti-myc-tag, MBL, 1:500 or rabbit anti-GST-π, MBL, 1:20,000) diluted in 3% NGS/PBST for overnight at 4 °C. The sections were then incubated with biotinylated goat anti-rabbit IgG (Vector Laboratories, Burlingame, CA) diluted 1:200 in 3% NGS/PBST for 1 h at RT, followed by the incubation for 30 min with avidin–biotin complex (ABC) reagent (ABC elite kit; Vector Laboratories) at RT. The peroxidase labeling was visualized with 3,3′-diaminobenzidine (DAB) substrate (Vector Laboratories) with or without nickel chloride.

For double immunostaining, after treated with Triton X-100 and H_2O_2 as above the sections were incubated in order with blocking reagents, primary antibody (mouse monoclonal anti-β-gal, Promega, Madison, WI; 1:1000 or mouse monoclonal anti-myc (9E10), Santa Cruz Biotechnology, Santa Cruz, CA, 1:1000), biotinylated anti-mouse IgG reagent and ABC reagent (Vector MOM peroxidase kit, Vector Laboratories) according to kit instructions except for incubation with primary antibody overnight at 4 °C. The 3-amino-9-ethylcarbazole (AEC, Sigma) was used to localize peroxidase and the sections were kept in PBS on ice. The immunoreactive cells in the cerebral cortex were viewed and photographed under light microscope (4× and 40× objective) connected with a color CCD camera (Olympus, Tokyo, Japan) to document the positions and morphologies of positive cells. Then sections were immersed in a graded ethanol series to eliminate AEC reaction product. After rehydrated and treated with 0.5% H_2O_2 to eliminate any residual peroxidase activity, the sections were incubated with rabbit polyclonal antibody to GST-π (MBL, 1:8000) for 5 days at 4 °C and labeled with ABC elite kit (Vector Laboratories) as described above, visualizing peroxidase with DAB-nickel (Vector Laboratories). The sections were dehydrated, cleared, and mounted.

The AEC reaction product was eliminated before the second immunostaining because cytoplasmic localization of β-gal or myc tagged GALC was largely overlapped with that of the second antigen GST-π and the dense AEC product appeared interfere with subsequent processes of immunostaining to detect GST-π. However, based on carefully documented anatomical locations including relation with nearest vessels and the morphologies of positive cells after immunostaining of the first antigen, the majority of doubly positive cells were easily identified after GST-π immunostaining (see Figs. 6G–J). Every third section at the levels corresponding to level 15–25 in the "Brain Maps: Structure of the Rat Brain" by Swanson [30] were used for morphological analysis of GST-π^+ cells and for untreated controls one section per animal at level 25 was used for the analysis. The morphology of the cells after GST-π staining was examined under microscope and photographed.

Immunofluorescence study

Tissues were prepared as described above and double immunofluorescence was performed as previously described [13]. The used primary antibodies were: mouse monoclonal anti-β-gal (Promega, 1:500), rabbit polyclonal anti-glial fibrillary acidic protein (GFAP; Dako, Glostrup, Denmark; 1:300), rabbit polyclonal anti-GST-π (MBL, 1:500) and rabbit polyclonal anti-myelin basic protein (MBP; Dako; 1:500). The secondary antibodies used were: rhodamine-conjugated goat anti-mouse IgG and FITC-conjugated goat anti-rabbit IgG (Cappel, Aurora, OH; 1:100). The sections were viewed under a fluorescence microscope and photographed using an AquaCosmos CCD camera (Hamamatsu Photonics, Hamamatsu, Japan).

Results

Determination of influence of ATG surrounding sequence to GALC activity

It is known that the sequence around the initiation codon in GALC gene is not optimal for translation according to Kozak rule [19–21]. Prior to the generation of recombinant retrovirus, to determine the sequence around initiation codon that gives rise to the most optimal expression of GALC, we generated three expression vectors carrying GALC cDNA with "original ATG," "Kozak ATG" and "1st ATG," respectively (Fig. 1). Transient expression studies ($n = 6$) in Bosc23, a cell line derived from the kidney of human embryo, showed no significant difference in GALC expression level among these three constructs. When expression study was performed in NIH/3T3 cells ($n = 3$), expression level from "original ATG" was higher than that of "Kozak ATG" or "1st ATG" with statistically significant difference (Fig. 2). The results indicate that pLHCAG (original) has comparable or better expression level than the other two constructs. And GALC gene with "original ATG" was used in subsequent study.

Epitope tagging of GALC gene

To favor the convenient identification of cells expressing transduced GALC gene in tissues, c-myc-epitope (1 or 3 copies) was introduced to the carboxyl-terminus of GALC with the "original ATG." In a pilot study, immunofluorescence against myc-tag after transfection showed that tandem three copies of the tag significantly improved signal strength comparing with a single copy

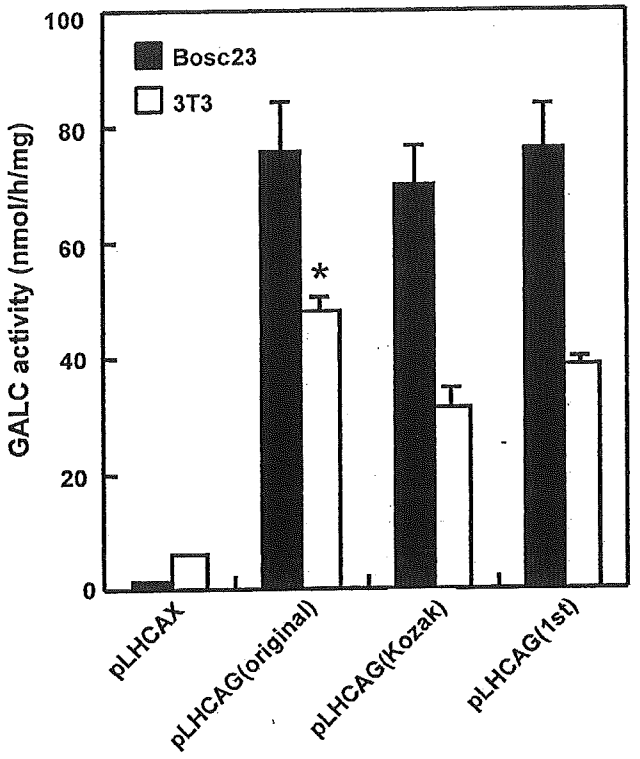

Fig. 2. Influence of ATG surrounding sequence to GALC activity. GALC activities in Bosc23 ($n = 6$) and NIH/3T3 ($n = 3$) cells transfected with retroviral vectors carrying GALC cDNA with "original ATG", "Kozak ATG" or "1st ATG." pLHCAX was used as control vector. The data are presented as mean ± SE *$P = 0.015$ and 0.038, ("original ATG" compared with "Kozak ATG" and "1st ATG" respectively, t test).

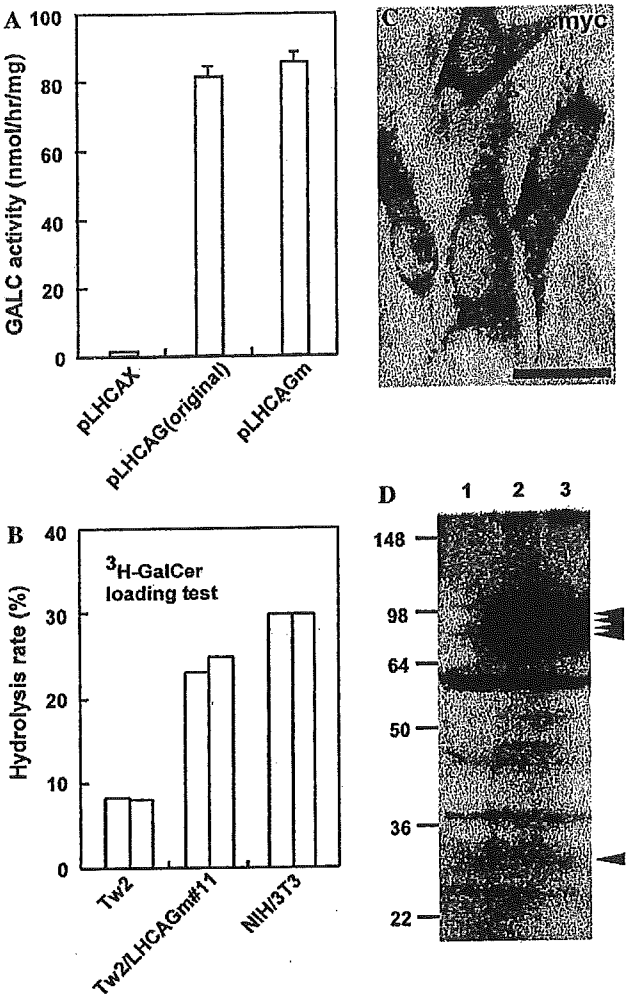

Fig. 3. Characterization of epitope tagged GALC protein. (A) GALC activities in Bosc23 ($n = 3$) transfected with retroviral vectors carrying GALC with (pLHCAGm) or without myc-tag (pLHCAG). pLHCAX was used as control vector. The data are presented as mean ± SE. (B) Hydrolysis rates of GalCer in twitcher fibroblasts (Tw2), a subclone of retrovirus LHCAGm-infected Tw2 (Tw2/LHCAGm#11) and NIH/3T3, assessed by [^{3}H]GalCer loading test ($n = 2$). (C) Myc-tag-immunocytochemistry in a subclone of ψMP34 stably transduced with pLHCAGm (ψMP34/pLHCAGm#92). Parental ψMP34 is a mouse fibroblasts-derived packaging cell line. (D) Western blot analysis of cell extracts from parental cell line ψMP34 (lane 1) and two subclones of ψMP34 stably transduced with pLHCAGm (ψMP34/pLHCAGm#92 and #96; lanes 2 and 3, respectively) labeled with rabbit antibody to the myc-tag. The molecular weight standards are shown on the left. Transgene-specific bands are indicated by arrowheads.

of tag, so the construct encoding GALC with triple epitope-tag (named as pLHCAGm, Fig. 1) was used subsequently to produce recombinant retrovirus.

It is critical to determine whether epitope-tag interferes with the normal structure and biological activity of GALC protein. Transient expression study showed that no decrement of GALC activity in the cells transfected with pLHCAGm comparing with the parent construct without epitope tagging (Fig. 3A). To further confirm that epitope tagging has no adverse effects on GALC, [^{3}H]GalCer loading test was carried out on a subclone of twitcher fibroblasts expressing myc-tagged-GALC (Tw2/LHCAGm#11;GALC activity: 14.07 nmol/h/mg). The hydrolysis rate of GalCer in Tw2/LHCAGm#11 significantly increased as compared with uninfected parental twitcher fibroblasts (Tw2), near that in NIH/3T3 cells (Fig. 3B). This demonstrated that GALC deficiency in the twitcher cells was restored by LHCAGm transduction and that epitope tagging has no influence on lysosomal targeting and intracellular catalytic activity of recombinant GALC protein.

Immunocytochemistry using antibody against myc-tag in cells stably transduced with pLHCAGm showed punctated stains throughout the cytoplasm (Fig. 3C). Western blot analysis of cell extracts from these cells showed transgene-specific bands between 80 and 90 kDa (four bands could be identified in shorter time of exposure) and one at about 30 kDa (Fig. 3D, arrowheads). The bands of 80–90 kDa may present the precursor form of GALC and the band near 30 kDa may present the C-terminal subunit of GALC [31–33]. The signal strength in 80–90 kDa was significantly stronger than that in 30 kDa suggesting that most of the immunoreactive signals observed in the immunocytochemical study above may be contributed to the precursor form of GALC protein.

Stable gene transfer to oligodendrocytes by SVZ injection of retrovirus

To transduce oligodendrocytes in vivo, we introduced retrovirus into the SVZ at neonatal period in the mouse. To investigate the pattern of gene transfer by SVZ injection, LHCAL was injected stereotactically into the SVZ of neonatal normal mice and the transduction pattern was examined by X-gal histochemistry and immunohistochemistry at P4 and P30. No noticeable inflammatory and other abnormality was observed in the brain. At P4, many β-gal$^+$ cells still remained in the SVZ and some positive cells were observed in the cortex and the white matter dorsal or lateral to the SVZ (Fig. 4A). At P30, when migration and differentiation of neural cells are almost completed in the mouse brain, β-gal$^+$ cells were scattered widely in the neocortex, subcortical white matter, and the striatum of the ipsilateral hemisphere (Fig. 4B). Few positive cells could be seen in the contralateral hemisphere. All transduced cells appeared to be glia and most of them could be classified into oligodendrocytes and astrocytes by morphological criteria described previously [26]. No β-gal$^+$ neuron could be found. Transduced oligodendrocytes were distributed both in the gray and white matter. In the white matter β-gal$^+$ oligodendrocytes had many longitudinal processes parallel to nerve fiber tract presumably the cytoplasmic tongues of myelin sheaths (Fig. 4C), while many transduced oligodendrocytes in the cerebral cortex showed abundant, tenuous processes corresponding to type I oligodendrocytes [34] (Fig. 4D). Most transduced astrocytes have protoplasmic morphology with highly branched feather-like processes (Fig. 4E). Cell type identification was further confirmed by double immunofluorescence using antibodies to both β-gal and cell type-specific markers (GFAP for astrocytes, GST-π and MBP for oligodendrocytes) (Figs. 4F and G).

The results were essentially consistent with earlier studies in rats [26] and demonstrated that SVZ injection of retrovirus in neonatal mouse is an ideal strategy to achieve persistent transduction of oligodendrocytes from early developmental stages.

Transduction of GALC to twitcher brain

GALC-expressing retrovirus LHCAGm was injected into the SVZ of twitcher mice at P0. Two out of 10 recipients disappeared at the next day and eight recipients survived at the time of analysis. No changes in the clinical symptoms such as small body, twitching and paralysis of hind limbs were observed in the LHCAGm injected twitcher mice comparing with untreated twitcher controls.

At P38–40, LHCAGm injected twitcher brains were studied for transgene expressing-cells by immunohistochemistry against myc-tag. Myc$^+$ cells were identified in four out of five examined twitcher brains. The distribution pattern of myc$^+$ cells in the brain sections was similar to that of β-gal$^+$ cells observed in the LHCAL injected normal mice described above. The number of myc$^+$ cells in the twitcher brain varies slightly among animals with an average number of ~10 cells in the cerebral cortex per section. All myc$^+$ cells were glial cells and most of them could be defined as either oligodendrocytes or astrocytes by their morphology. The transduced

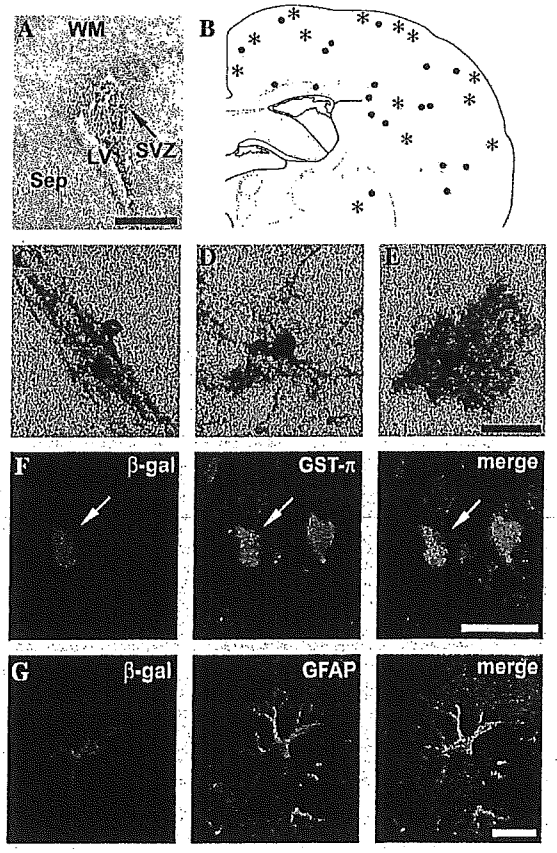

Fig. 4. Gene transfer to the brain of normal mouse by SVZ injection of LHCAL. (A) X-gal stained coronal brain section at P4 shows many β-gal$^+$ cells (blue) located in the SVZ. The level of the section nears the site of injection. (B) Schematic representation of the distribution of β-gal$^+$ cells based on immunostaining to β-gal in the recipient's brain at P30. Closed circles and asterisks represent positive oligodendrocytes and astrocytes respectively. (C–E) Microscopic photographs of β-gal-immunoreactive glial cells in the recipients brain at P30. (C) A positive oligodendrocyte in the white matter. Note immunoreactive longitudinal processes parallel to the nerve tract. (D) An immunoreactive oligodendrocyte in the cerebral cortex. (E) A positive protoplasmic astrocyte in the cerebral cortex. (F and G) Cell-type identification of transduced cells by double immunofluorescence. (F) A β-gal-immunoreactive cell (red) in the cerebral cortex was GST-π$^+$ (green), indicating it is an oligodendrocyte. (G) Two β-gal-immunoreactive cells (red) in the cerebral cortex were GFAP$^+$ (green), indicating they are astrocytes. The two cells contact closely suggesting they may be daughters of the same progenitor. LV, lateral ventricle; WM, white matter; Sep, septum; SVZ, subventricular zone. The schema of the brain in (B) was adopted from "Brain Maps: Structure of the rat Brain" by Swanson [30]. Scale bar: 250 μm in (A); 25 μm in (C–E); 20 μm in (F and G). (For interpretation of the references to colors in this figure legend, the reader is referred to the web version of this paper.)

oligodendrocytes exhibited an intense cytoplasmic staining with moderately stained asymmetrical nucleus (Fig. 6E). Only a few proximal processes extended from cell body could be identified in LHCAGm transduced oligodendrocytes. Myc$^+$ astrocytes exhibited stains in the rim of cytoplasm and abundant bushy processes with relatively pale nucleus (Fig. 6F).

The presence and expression of transduced GALC gene in the recipient twitcher brain was analyzed by PCR and RT-PCR using primers specific for human GALC at P35–39 (Fig. 5). All three twitcher recipients' brains examined were positive for human GALC cDNA (provirus DNA) and human GALC transcript. The authenticity of the PCR product was confirmed by Southern blot with a human GALC probe. GALC expression was further assessed by enzymatic assay. There was no measurable GALC activities in the transduced twitcher brain above untreated twitcher controls (GALC activities: 0.05 ± 0.01, 0.08 ± 0.01, and 2.24 ± 0.14 nmol/h/mg in transduced twitcher, age-matched untreated twitcher and untreated normal mouse brain, respectively, each three animals). This was not unexpected since the number of transduced cells in the brain was very small. The activity of transduced GALC in the whole brain homogenate may be under the detection limit of this enzyme assay system.

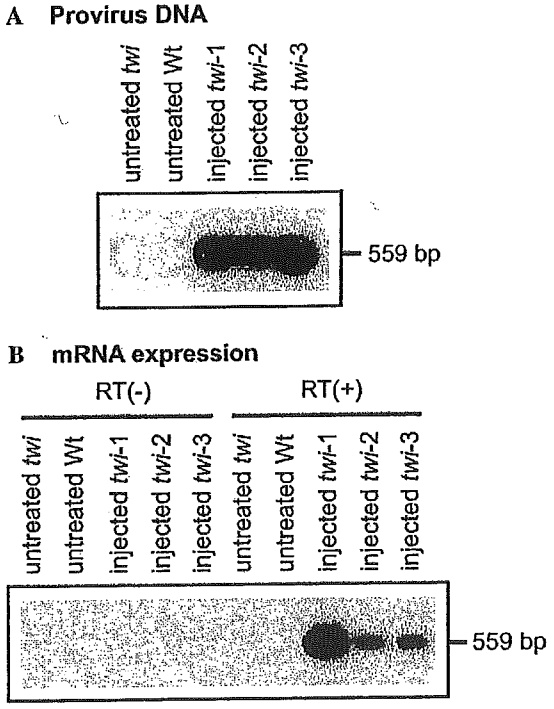

Fig. 5. Presence and expression of transduced human GALC in the twitcher brains which received neonatal SVZ injection of LHCAGm. Southern blot analysis. (A) PCR amplification of genomic DNA from the whole brain to detect the presence of the integrated provirus. (B) Human GALC transcript was detected by RT-PCR using total RNA from the whole brain. The authenticity of PCR products was confirmed by hybridized with a human GALC probe. RT (+) and RT (−) indicate amplified PCR products form cDNA samples with and without reverse transcriptase, respectively.

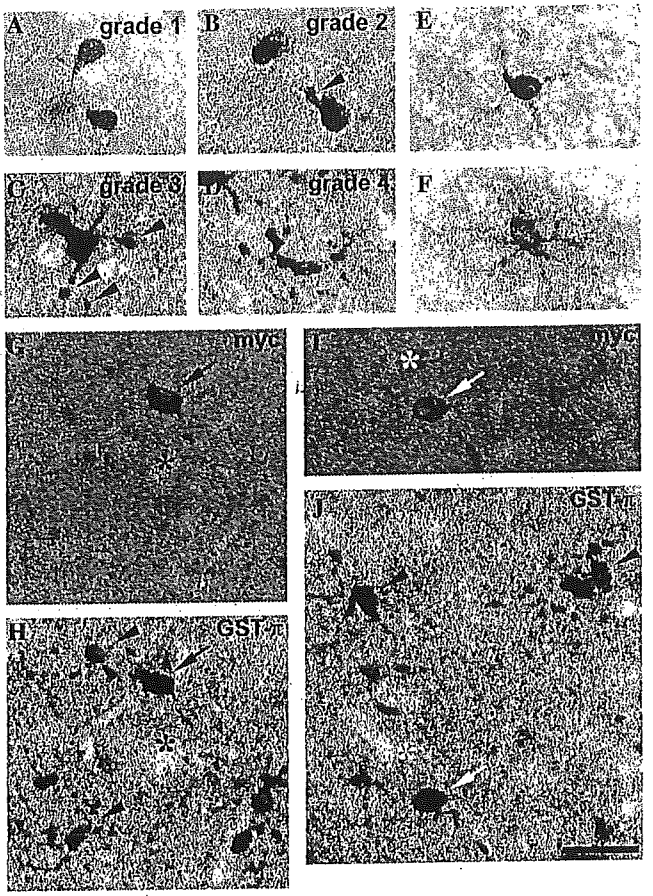

Fig. 6. Morphological correction of twitcher oligodendrocytes by GALC transduction. (A–D) The severity of morphological aberrations of oligodendrocytes in the cerebral cortex was divided into four grades by GST-π-immunostaining. (E and F) LHCAGm transduced oligodendrocyte (E) and astrocyte (F) in the twitcher cerebral cortex at around P40, identified by immunohistochemistry against myc-tag. (G and H) A representative brain section from LHCAGm injected twitcher cerebral cortex subsequently stained with mouse anti-myc-tag (G, chromogen: AEC) and rabbit anti-GST-π (H, chromogen: DAB-$NiCl_2$) antibodies. A myc$^+$/GST-π$^+$ cell (arrow) exhibits normal morphology (Grade 1), while myc$^-$/GST-π$^+$ cells (arrowheads) show severe aberrant morphologies (Grades 3 and 4). Asterisk indicates the blood vessel nearing myc$^+$ cell as anatomic marker. (I and J) Another brain section stained with anti-myc (I) and anti-GST-π (J) antibodies. Scale bar: 20 μm.

Morphological improvements in GALC transduced oligodendrocytes in the twitcher brain

To evaluate the effects of GALC transduction on the morphology of oligodendrocytes, an analysis using combined immunostaining for myc-epitope and GST-π was carried out. GST-π has been well documented as a marker of oligodendrocytes [35] and previously used to investigate morphological aberrations in twitcher oligodendrocytes [8]. Unlike many other oligodendroglial markers such as MBP, 2′,3′ -cyclic nucleotide

3′-phosphodiesterase (CNPase), and proteolipid protein (PLP) that mainly stain the processes of oligodendrocytes and myelin, GST-π clearly reveals the cell soma and some processes and appears suitable for morphological investigation of oligodendrocytes.

Oligodendroglial morphology was examined in the cerebral cortex since unlike those in the white matter oligodendrocytes in the cerebral cortex is less compact distributed which makes the morphological examination much easier to perform. To quantitatively evaluate the aberrations in the morphology of oligodendrocytes, the severity of morphological changes were divided to four grades based on their morphologies in the normal and untreated twitcher mice at P40 after GST-π-immunostaining: Grade 1, spherical, oval or slightly polygonal soma (Fig. 6A). This is typical normal morphology and almost all oligodendrocytes in the normal mouse show this morphology. Grade 2, slightly polygonal soma with one or two swelling-like structures (Fig. 6B, arrowhead) at the soma or the proximal processes. This morphology may be abnormal but could also be seen in oligodendrocytes of the normal mouse at low frequency, so it represents normal or slightly abnormal morphology. Grade 3, markedly altered morphology including enlarged soma, irregularly thick processes and various sizes of swellings at different sites of the processes (Fig. 6C, arrowheads). The morphologies of this grade are never seen in oligodendrocytes of the normal mouse, while most oligodendrocytes in the twitcher at P40 show these morphologies. Grade 4, severe aberrant morphology with shrunken soma and/or fragmented processes (Fig. 6D). Oligodendrocytes displaying this morphology probably correspond to the apoptotic oligodendrocytes described previously [8].

The summary of morphological analysis of oligodendrocytes was shown in Table 1. Around P40, more than 93% of the cerebral cortical oligodendrocytes (GST-π^+ cells) in the untreated twitcher mice showed severe aberrant morphologies (Grade 3–4) (Figs. 6C and D). As viral infection controls, neonatal twitcher mice received LHCAL injection were analyzed for morphologies of transduced oligodendrocytes (β-gal$^+$/GST-π^+ cells) at P38–39. More than 86% β-gal$^+$/GST-π^+ cells in these mice had severe abnormal morphology (Grade 3–4). This suggests that virus vector injection itself does not alter the morphology of oligodendrocytes in the twitcher mice.

In contrast, dramatic morphological improvement in oligodendrocytes was observed in the twitcher mice that received LHCAGm. About 83% of GALC expressing-oligodendrocytes (myc$^+$/GST-π^+ cells) exhibited completely normal morphology (Grade 1) (arrows in Figs. 6G–J). Only less than 5% of myc$^+$/GST-π^+ cells had typical abnormal morphology such as swellings at the soma or processes (Grade 3). And none was classified to Grade 4. The percentages of cells of each grade within myc$^+$/GST-π^+ cells in these mice were significantly different from that in untreated twitcher mice or twitcher mice received LHCAL injection ($P<0.0001$, χ^2 test). Despite the significant normalization of myc$^+$ oligodendrocytes in LHCAGm transduced twitcher mice, the untransduced (myc-negative) oligodendrocytes located nearing showed aberrations in morphology (arrowheads in Figs. 6H and J). When morphological analysis was performed on GST-π^+ cells in the cerebral cortex of these mice regardless of myc-immunoreactivity, the percentages of cells of each grade were undistinguishable from those in untreated twitcher controls. This indicates that the persistent expression of GALC in a small number of glial cells did not result in diffuse correction of neighboring oligodendrocytes in the twitcher brain.

Discussion

At present hematopoietic stem cell transplantation is the only available treatment for GLD, especially the late-onset form [4]. At the mean time, gene therapy is another promising strategy to treat inherited disorders like GLD which results from mutations of a single gene. Basic studies on the understanding of the effects of transduced GALC in myelin-forming cells are important in the assessment of the potential of gene therapy in GLD. Previous experiments that introduced GALC gene into cultured oligodendrocytes derived from twitcher showed appropriate localization of the enzyme and normal morphology with highly branched processes in some transduced oligodendrocytes [16,17]. In the present study, an in vivo model for transducing oligodendro-

Table 1
Morphological analysis of oligodendrocytes in the cerebral cortex

Morphological grading	Wild type	Untreated twitcher	Twitcher-LHCAL	Twitcher-LHCAGm	
	GST-π^+ ($n=3$)	GST-π^+ ($n=4$)	β-gal$^+$/GST-π^+ ($n=3$)	myc$^+$/GST-π^+ ($n=4$)	GST-π^+ ($n=3$)
1	99.6 ± 0.3% (3281)	1.8 ± 0.3% (28)	5.3 ± 1.9% (10)	83.5 ± 1.3% (101)	1.0 ± 0.3% (19)
2	0.4 ± 0.3% (14)	4.4 ± 1.2% (69)	8.6 ± 1.2% (19)	11.9 ± 1.2% (15)	3.2 ± 0.9% (60)
3	0% (0)	85.8 ± 1.5% (1385)	73.8 ± 0.8% (160)	4.6 ± 1.2% (5)	87.8 ± 1.1% (1708)
4	0% (0)	8.1 ± 1.3% (132)	12.3 ± 1.3% (28)	0% (0)	8.0 ± 1.3% (154)
Total	100% (3295)	100% (1614)	100% (217)	100% (121)	100% (1941)

Data is presented as mean ± SE. In parentheses are the sums of cell numbers counted from 3 or 4 animals.

cytes with GALC was developed and results showed that the morphology was completely corrected in most of the transduced twitcher oligodendrocytes. This suggested that GALC may play an important role in the maintenance of the normal morphology of oligodendrocytes in vivo and provided direct evidence for the usefulness of gene therapy in GLD.

It is known that many lysosomal enzymes can be secreted from normal cells and taken up by enzyme-deficient cells, and this process, called cross-correction, occurs either by direct cell-to-cell transfer or cell surface receptor-mediated endocytosis. Cross-correction is an important concept in gene therapy strategies to treat lysosomal storage diseases since the non-transduced affected cells could also be corrected by this mechanism. And it is also the rationale for the use of hematopoietic stem cell or intracerebral cell transplantation in treating lysosomal diseases that affects the CNS such as Krabbe disease. Previous studies demonstrated that GALC can be secreted into culture medium from normal or over-expressing cells and can be incorporated by several types of enzyme-deficient cells including oligodendrocytes, astrocytes and Schwann cells in vitro [17,36,37]. In the present study, we initially expected that positive signal could be detected in the neural cells neighboring the transduced cells. However, the myc-tag-immunostaining in the brain always showed sharp boundaries between positive and negative cells and we could not observe traces of immunoreactive signals in the brain cells neighbor, even adjacent to positive glial cells above background (Figs. 6G and I). Moreover, despite of the significant morphological correction of myc$^+$ twitcher oligodendrocytes, we could not observe phenotypic changes in oligodendrocytes located nearing positive oligodendrocytes (e.g., the cell on the left upper hand of Fig. 6H pointed by arrowhead). Thus we did not obtain histological evidence for cross-correction of GALC in vivo. However, we cannot rule out the possibility that the level of GALC expression in vivo in our study was relatively low and the amount of enzyme supplied to surrounding cells was insufficient to achieve morphological restoration or to be detected by the immunostaining. Another possible reason could be that the cross-correction process of human GALC is insufficient in the mouse cells. For this, a specifically designed study should be needed to determine the evidence and implications of cross-correction of GALC in vivo.

Stable transduction of oligodendrocytes is essential for successful examination of the in vivo effects of the transgene. To transduce oligodendrocytes, we chose SVZ injection of retrovirus at neonatal period. This is because that in murine, gliogenesis takes place largely in early postnatal life and most oligodendroglial progenitor cells are located in the SVZ at neonatal period. These mitotically active progenitor cells could be infected by retrovirus, migrate away from the SVZ and differentiate into mature oligodendrocytes. Results showed that the neonatal injection of retrovirus into SVZ has significant advantages over direct injection of viral vectors into brain parenchyma to transduce mature oligodendrocytes. The latter usually transduces various types of cells concentrated at the injection sites and leads to obvious trauma and inflammatory reactions making the morphological analysis difficult to perform. Comparing with the infectious titer of LHCAGm the transduction level in this study was low (up to 10 myc$^+$ cells were observed in the cerebral cortex per section). The presence of inhibitory factors (non-transducing viral particles and free viral envelope proteins) in the viral stocks may be one of the reasons for the discrepancy between the low in vivo transfectability and the viral titer [38].

Sensitive localization of the protein products of transgene in vivo is an important issue in evaluating the effects of the transgene. Although polyclonal antibodies against GALC have been used to identify GALC-expressing cells in culture systems and tissues previously [17,39], our results showed epitope tagging is also useful. Immunohistochemistry using commercially available antibodies to myc-tag gave to sensitive detection of transduced GALC with satisfactory signal-to-noise ratio in the brain tissues. Epitope-tags at the C-terminus of GALC protein did not interfere with lysosomal targeting and the bioactivity of transduced GALC as demonstrated by transient expression study and [^{3}H]GalCer loading study. Since the antibodies to epitope-tag are specific to the product of the transgene and do not cross-react with endogenous GALC, this method will particularly be useful in gene therapy experiments using normal cells or animals and the patient's cells that produce enzymatically defective but antigenic GALC protein.

Previous studies suggested that GALC protein is synthesized as 80–90 kDa precursor which is then cleaved to yield the 50 and 30 kDa subunits [19,20,31–33]. Consistently, cell extracts of transduced mouse fibroblasts in this study also showed bands at 80–90 and 30 kDa in Western blot analysis. However, the signal of the band near 30 kDa was very weak comparing with bands at 80–90 kDa. Two possible explanations of this finding are: (i) After the precursor being cleaved to 50 and 30 kDa subunits, the myc-epitope was removed from 30 kDa subunit either through proteolytic cleavage at the carboxyl terminus or non-specific degradation. (ii) Precursor form of human GALC protein could not be effectively cleaved to two subunits in the mouse fibroblasts because of species-specific or cell type-specific processing. Further experiments such as Western blot analysis of cell extracts using antibodies recognizing GALC protein or enzyme assay on lysosomal fraction from these cells is needed to clarify this question.

Transfection study in Bosc23 and NIH/3T3 cells showed that "original ATG" gave rise to similar or higher level of expression of GALC than "Kozak ATG"

or "1st ATG." While Chen et al. [19] have reported that modification of the sequences surrounding the initiation codon to more consensus one (A in position +4 to G) resulted in improved expression of GALC in COS-1 cells. This discrepancy suggested that although the sequence around the initiation codon in GALC gene is not optimal for translation according to Kozak rule, when GALC cDNA was driven by a strong heterologous promoter the expression level may be largely influenced by expression vectors and the host cell types rather than ATG surrounding sequence. In our earlier study [37], we reported higher GALC expression in "Kozak ATG" than "original ATG" as unpublished data, however by repeated experiments thereafter we found it should be revised.

Taken together, introduction of retrovirus into the SVZ of neonatal twitcher mouse resulted in stable transduction and expression of GALC in twitcher oligodendrocytes as analyzed by RT-PCR and immunohistochemistry and significant phenotypic improvements were achieved in these transduced oligodendrocytes. Obviously, the morphological aberrations and degeneration of twitcher oligodendrocytes in the CNS [7,8,40] or in culture systems [41,42] are caused by metabolic perturbation most likely the accumulation of psychosine, thus, morphological correction of transduced oligodendrocytes in this study probably reflects normalized biological functions of these cells. Further studies will be conducted to investigate whether and how these morphological corrections are related to functional improvements and myelin sheath preservation. We believe these basic studies will be useful for the development of future gene therapy approaches to treat this severe and fatal leukodystrophy.

Acknowledgments

We thank Kazuhiro Ikenaka (Department of Neural Information, National Institute for Physiological Sciences, Okazaki, Japan) and Tadanori Yoshimatsu (Institute for Biotechnology Research, Wakunaga Pharm., Hiroshima, Japan) for kindly providing the packaging cell line ψMP34 [24] and Masato Matsushima (Division of Clinical Research & Development, The Jikei University School of Medicine) for valuable advise on statistical analysis and Ryozo Gotoh (Laboratory Animal Center, The Jikei University School of Medicine) for technical assistance.

References

[1] D.A. Wenger, K. Suzuki, Y. Suzuki, K. Suzuki, Galactosylceramide lipidosis: globoid cell leukodystrophy (Krabbe disease), in: C.R. Scriver, A.L. Beaudet, W.S. Sly, D. Valle (Eds.), The Metabolic and Molecular Bases of Inherited Disease, McGraw-Hill, New York, 2001, pp. 3669–3694.

[2] T. Miyatake, K. Suzuki, Globoid cell leukodystrophy: additional deficiency of psychosine galactosidase, Biochem. Biophys. Res. Commun. 48 (1972) 538–543.

[3] K. Suzuki, Twenty-five years of the psychosine hypothesis: a personal perspective of its history and present status, Neurochem. Res. 23 (1998) 251–259.

[4] W. Krivit, E.G. Shapiro, C. Peters, J.E. Wagner, G. Cornu, J. Kurtzberg, D.A. Wenger, E.H. Kolodny, M.T. Vanier, D.J. Loes, K. Dusenbery, L.A. Lockman, Hematopoietic stem-cell transplantation in globoid-cell leukodystrophy, N. Engl. J. Med. 338 (1998) 1119–1126.

[5] K. Suzuki, K. Suzuki, The twitcher mouse: a model for Krabbe disease and for experimental therapies, Brain Pathol. 5 (1995) 249–258.

[6] N. Sakai, K. Inui, N. Tatsumi, H. Fukushima, T. Nishigaki, M. Taniike, J. Nishimoto, H. Tsukamoto, I. Yanagihara, K. Ozono, S. Okada, Molecular cloning and expression of cDNA for murine galactocerebrosidase and mutation analysis of the twitcher mouse, a model of Krabbe's disease, J. Neurochem. 66 (1996) 1118–1124.

[7] S.M. LeVine, M.V. Torres, Morphological features of degenerating oligodendrocytes in twitcher mice, Brain Res. 587 (1992) 348–352.

[8] M. Taniike, I. Mohri, N. Eguchi, D. Irikura, Y. Urade, S. Okada, K. Suzuki, An apoptotic depletion of oligodendrocytes in the twitcher, a murine model of globoid cell leukodystrophy, J. Neuropathol. Exp. Neurol. 58 (1999) 644–653.

[9] A.M. Yeager, S. Brennan, C. Tiffany, H.W. Moser, G.W. Santos, Prolonged survival and remyelination after hematopoietic cell transplantation in the twitcher mouse, Science 225 (1984) 1052–1054.

[10] P.M. Hoogerbrugge, K. Suzuki, K. Suzuki, B.J. Poorthuis, T. Kobayashi, G. Wagemaker, D.W. van Bekkum, Donor-derived cells in the central nervous system of twitcher mice after bone marrow transplantation, Science 239 (1988) 1035–1038.

[11] K. Suzuki, P.M. Hoogerbrugge, B.J. Poorthuis, D.W. Bekkum, K. Suzuki, The twitcher mouse. Central nervous system pathology after bone marrow transplantation, Lab. Invest. 58 (1988) 302–309.

[12] D.A. Wenger, E.Y. Snyder, R.M. Taylor, M.T. Vanier, M.A. Rafi, P. Luzi, J. Datto, Neural stem cells for the treatment of the twitcher mouse model of Krabbe disease, Am. J. Hum. Genet. 65 (1999) A116.

[13] J.S. Shen, K. Watabe, T. Ohashi, Y. Eto, Intraventricular administration of recombinant adenovirus to neonatal twitcher mouse leads to clinicopathological improvements, Gene Ther. 8 (2001) 1081–1087.

[14] C. Fantz, D.A. Wenger, M. Sands, Neonatal and in utero gene transfer utilizing adeno-associated virus and lentiviral vectors for the treatment of Krabbe's disease, Mol. Ther. 3 (2001) S228.

[15] Y.P. Wu, E.J. McMahon, J. Matsuda, K. Suzuki, G.K. Matsushima, K. Suzuki, Expression of immune-related molecules is down-regulated in twitcher mice following bone marrow transplantation, J. Neuropathol. Exp. Neurol. 60 (2001) 1062–1074.

[16] E. Costantino-Ceccarini, A. Luddi, M. Volterrani, M. Strazza, M.A. Rafi, D.A. Wenger, Transduction of cultured oligodendrocytes from normal and twitcher mice by a retroviral vector containing human galactocerebrosidase (GALC) cDNA, Neurochem. Res. 24 (1999) 287–293.

[17] A. Luddi, M. Volterrani, M. Strazza, A. Smorlesi, M.A. Rafi, J. Datto, D.A. Wenger, E. Costantino-Ceccarini, Retrovirus-mediated gene transfer and galactocerebrosidase uptake into twitcher glial cells results in appropriate localization and phenotype correction, Neurobiol. Dis. 8 (2001) 600–610.

[18] G.K. Matsushima, M. Taniike, L.H. Glimcher, M.J. Grusby, J.A. Frelinger, K. Suzuki, J.P. Ting, Absence of MHC class II molecules reduces CNS demyelination, microglial/macrophage infiltra-

tion, and twitching in murine globoid cell leukodystrophy, Cell 78 (1994) 645–656.
[19] Y.Q. Chen, M.A. Rafi, G. de Gala, D.A. Wenger, Cloning and expression of cDNA encoding human galactocerebrosidase, the enzyme deficient in globoid cell leukodystrophy, Hum. Mol. Genet. 2 (1993) 1841–1845.
[20] N. Sakai, K. Inui, N. Fujii, H. Fukushima, J. Nishimoto, I. Yanagihara, Y. Isegawa, A. Iwamatsu, S. Okada, Krabbe disease: isolation and characterization of a full-length cDNA for human galactocerebrosidase, Biochem. Biophys. Res. Commun. 198 (1994) 485–491.
[21] M. Kozak, The scanning model for translation: an update, J. Cell Biol. 108 (1989) 229–241.
[22] N. Sakai, H. Fukushima, K. Inui, L. Fu, T. Nishigaki, I. Yanagihara, N. Tatsumi, K. Ozono, S. Okada, Human galactocerebrosidase gene: promoter analysis of the 5′-flanking region and structural organization, Biochim. Biophys. Acta 1395 (1998) 62–67.
[23] J.S. Shen, X.L. Meng, T. Yokoo, K. Sakurai, K. Watabe, T. Ohashi, Y. Eto, Widespread and highly persistent gene transfer to the CNS by retrovirus vector in utero: implication for gene therapy to Krabbe disease, J. Gene Med. (in press).
[24] T. Yoshimatsu, M. Tamura, S. Kuriyama, K. Ikenaka, Improvement of retroviral packaging cell lines by introducing the polyomavirus early region, Hum. Gene Ther. 9 (1998) 161–172.
[25] N.E. Bowles, R.C. Eisensmith, R. Mohuiddin, M. Pyron, S.L. Woo, A simple and efficient method for the concentration and purification of recombinant retrovirus for increased hepatocyte transduction in vivo, Hum. Gene Ther. 7 (1996) 1735–1742.
[26] S.W. Levison, J.E. Goldman, Both oligodendrocytes and astrocytes develop from progenitors in the subventricular zone of postnatal rat forebrain, Neuron 10 (1993) 201–212.
[27] S. Raghavan, A. Krusell, Optimal assay conditions for enzymatic characterization of homozygous and heterozygous twitcher mouse, Biochim. Biophys. Acta 877 (1986) 1–8.
[28] T. Kobayashi, N. Shinnoh, Y. Kuroiwa, Metabolism of galactosylceramide in the twitcher mouse, an animal model of human globoid cell leukodystrophy, Biochim. Biophys. Acta 879 (1986) 215–220.
[29] T. Kobayashi, N. Shinnoh, Y. Kuroiwa, Metabolism of ceramide trihexoside in cultured skin fibroblasts from Fabry's patients, carriers and normal controls, J. Neurol. Sci. 65 (1984) 169–177.
[30] L.W. Swanson, Brain Maps: Structure of the Rat Brain, Elsevier Science, Amsterdam, 1998.
[31] Y.Q. Chen, D.A. Wenger, Galactocerebrosidase from human urine: purification and partial characterization, Biochim. Biophys. Acta 1170 (1993) 53–61.
[32] N. Sakai, K. Inui, M. Midorikawa, Y. Okuno, S. Ueda, A. Iwamatsu, S. Okada, Purification and characterization of galactocerebrosidase from human lymphocytes, J. Biochem. (Tokyo) 116 (1994) 615–620.
[33] S. Nagano, T. Yamada, N. Shinnoh, H. Furuya, T. Taniwaki, J. Kira, Expression and processing of recombinant human galactosylceramidase, Clin. Chim. Acta 276 (1998) 53–61.
[34] S. Szuchet, The morphology and ultrastructure of oligodendrocytes and their functional implications, in: H. Kettenmann, B.R. Ransom (Eds.), Neuroglia, Oxford University Press, New York, 1995, pp. 23–43.
[35] F.A. Tansey, W. Cammer, A pi form of glutathione-*S*-transferase is a myelin- and oligodendrocyte-associated enzyme in mouse brain, J. Neurochem. 57 (1991) 95–102.
[36] M.A. Rafi, J. Fugaro, S. Amini, P. Luzi, G. de Gala, T. Victoria, C. Dubell, M. Shahinfar, D.A. Wenger, Retroviral vector-mediated transfer of the galactocerebrosidase (GALC) cDNA leads to overexpression and transfer of GALC activity to neighboring cells, Biochem. Mol. Med. 58 (1996) 142–150.
[37] J.S. Shen, K. Watabe, X.L. Meng, H. Ida, T. Ohashi, Y. Eto, Establishment and characterization of spontaneously immortalized Schwann cells from murine model of globoid cell leukodystrophy (twitcher), J. Neurosci. Res. 68 (2002) 588–594.
[38] S.P. Forestell, E. Bohnlein, R.J. Rigg, Retroviral end-point titer is not predictive of gene transfer efficiency: implications for vector production, Gene Ther. 2 (1995) 723–730.
[39] R. De Gasperi, V.L. Friedrich, G.M. Perez, E. Senturk, P.H. Wen, K. Kelley, G.A. Elder, M.A. Gama Sosa, Transgenic rescue of Krabbe disease in the twitcher mouse, Gene Ther. 11 (2004) 1188–1194.
[40] H. Takahashi, H. Igisu, K. Suzuki, K. Suzuki, The twitcher mouse: an ultrastructural study on the oligodendroglia, Acta Neuropathol. (Berl) 59 (1983) 159–166.
[41] H. Nagara, H. Ogawa, Y. Sato, T. Kobayashi, K. Suzuki, The twitcher mouse: degeneration of oligodendrocytes in vitro, Brain Res. 391 (1986) 79–84.
[42] H. Ida, F. Kawame, S.U. Kim, Y. Eto, Abnormality in cultured oligodendrocytes and Schwann cells isolated from the twitcher mouse, Mol. Chem. Neuropathol. 13 (1990) 195–204.

Exp. Anim. 55(1), 65–69, 2006

—Note—

Transgene Insertion Pattern Analysis Using Genomic Walking in a Transgenic Mouse Line

Osamu SUZUKI*, Tomoko HATA, Naho TAKEKAWA, Minako KOURA*, Kaoru TAKANO*, Yoshie YAMAMOTO, Yoko NOGUCHI*, Kozue UCHIO-YAMADA*, and Junichiro MATSUDA*

Department of Veterinary Science, National Institute of Infectious Diseases, 1–23–1 Toyama, Shinjuku-ku, Tokyo 162-8640, Japan
**Current address: Laboratory of Experimental Animal Models, National Institute of Biomedical Innovation, 7–6–8 Saitoasagi, Ibaraki-shi, Osaka 567-0085, Japan*

Abstract: *A transgene mapping technique (Noguchi* et al., *Exp. Anim. 53:103-111, 2004) is described that can be used to analyze transgene integration patterns in transgenic mice. The technique was used to reveal that a transgenic mouse line (GM1-sy#116) harbored inverted and direct tandem repeats of both intact and partial pCAGGS-based transgenes in the G2 region of chromosome 1. This complicated concatenation of transgenes may have been caused by simple end-joining of DNA constructs fragmented by exposure to UV transillumination during gel-purification, and by nuclease digestion inside zygote pronuclei. The results suggest that care should be taken to avoid unwanted fragmentation during the preparation of vector constructs.*

Key words: *genomic walking, integration pattern, transgene*

Simple and accurate genotyping methods, especially those designed to assess zygosity, are necessary for the efficient use and management of transgenic laboratory animals. In a previous report, we described a simple and efficient method for genetic mapping and zygosity analysis of transgenes [12]. Sequences flanking the trangenes are determined using genomic walking, which allows the transgene insertion sites in chromosomes to be located by searching a genome database. In addition, flanking primers can be designed to assess the zygosity of the transgene loci in transgenic animals using PCR [10]. Here, we report that the genomic walking technique can be used to determine the transgene insertion pattern, as well as the flanking sequences, and we discuss the mechanism of transgene integration into chromosomes.

We used a transgenic mouse line, GM1-sy#116, with a C57BL/6JJmsSlc background, which was produced in our laboratory by zygote microinjection of transgene constructs based on a pCAGGS plasmid [11]. The constructs (Fig. 1A) consisted of fragments generated from the *SalI–Hin*dIII site of plasmid pCAGGS, which contains a ganglioside GM1 synthase cDNA [5] cloned in our laboratory from C57BL/6J genomic DNA. All ani-

(Received 4 July 2005 / Accepted 26 September 2005)
Address corresponding: O. Suzuki, Laboratory of Experimental Animal Models, National Institute of Biomedical Innovation, 7–6–8 Saitoasagi, Ibaraki-shi, Osaka 567-0085, Japan

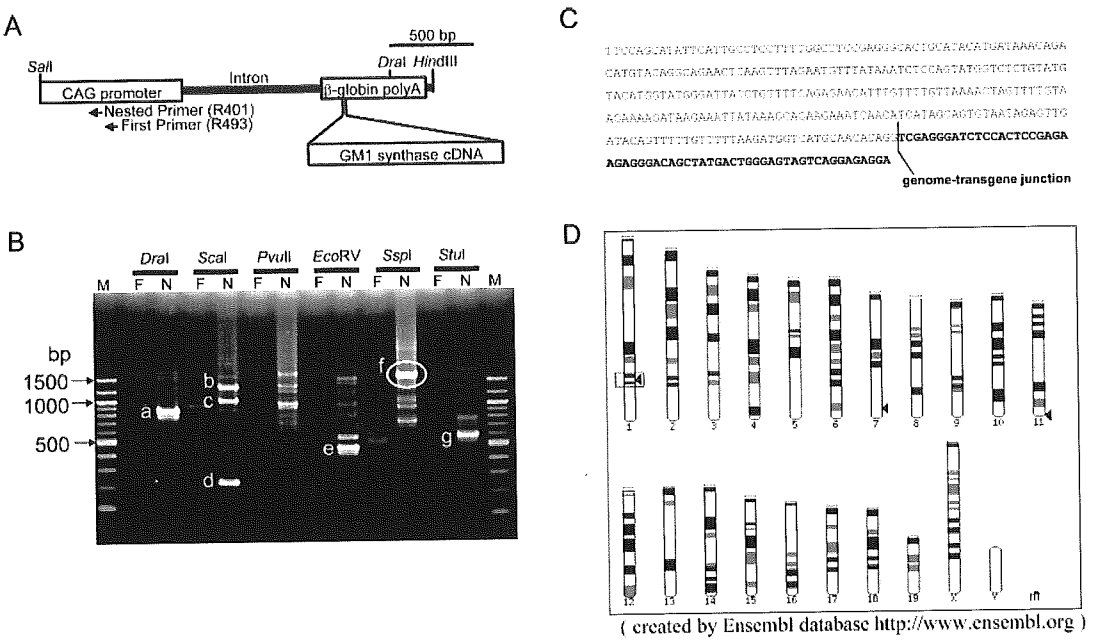

Fig. 1. Chromosomal mapping in the transgenic mouse line GM1sy#116. The integrated transgene construct contained GM1 synthase cDNA (A). The products of first (F) and nested (N) PCR amplifications using GM1sy#116 genomic libraries were separated by agarose gel electrophoresis (B). The sequence (C) flanking the transgene was determined using an approximately 1.5-kb band amplified from an *Ssp*I library (band f in B). Other bands (a-e and g) did not provide flanking sequence information. A search of the Ensembl genome database using the flanking sequence, under the condition *Expectation value* < 0.001, located the transgene to the G2 region of chromosome 1 (boxed in D). M, 100-bp DNA ladder.

mal experiments were performed according to the Guides for Animal Experiments Performed at the NIID.

The sequences around the transgenes were determined by genomic walking using the method described previously [12], but with different transgene-specific primers, R493 (CCG CCC CCA TCG CTG CAC AAA ATA AT) and R401 (GTG GGG CTC ACC TCG ACC CAT GGT AAT). Some of the PCR amplicons (bands a–g in Fig. 1B) were gel-purified and sequenced directly using a DYEnamic ET Terminator Cycle Sequencing Kit (Amersham Biosciences, Piscataway, NJ, USA) with a DNA sequencer (RISA384, Shimadzu Biotech, Kyoto, Japan). The transgene insertion sites in the chromosomes were determined by BLAST search in the Ensembl genome database [9] of the sequences flanking the transgene (Fig. 1C). Searches were conducted over the Internet (http://www.ensembl.org), and were based on the mouse genome assembly NCBI build m33 (Fig. 1D).

Sequences of both transgene-genomic junctions were confirmed by PCR analyses using the flanking primer method. Two flanking primers, designated S412 (CAT GGT ATG GGA TTA CCT GTT TTC AGA) and R677 (CCC GGG CCC CAC ACT CAG AAC CTC TCT; Fig. 2A), were designed with the Primer3 program [15], using the flanking sequence around the transgene retrieved from the Ensembl database. A primer for the 3'-tail of the construct was also designed (pCAG-S2238; CCC TCT TCT CTT ATG AAG ATC CCT CGA CCT). PCR product formation was checked by PCR with tail DNA from transgenic mice and three combinations of primers (Fig. 2B): pCAG-S2238 only; pCAG-S2238 and S412; and pCAGGS-S2238 and R677. The zygosities of homozygous transgenic, hemizygous transgenic, and non-transgenic animals were determined by PCR of their tail DNA, the flanking primers, and pCAG-S2238 (Fig. 2C). Both PCR analyses were done under the following thermal conditions: 95°C for 15 min, followed by 30 cycles of 94°C for 5 s, 60°C for 5 s, and 72°C for 30 s. All PCR amplifications, including the genomic walking analysis, were conducted using a hot-start DNA

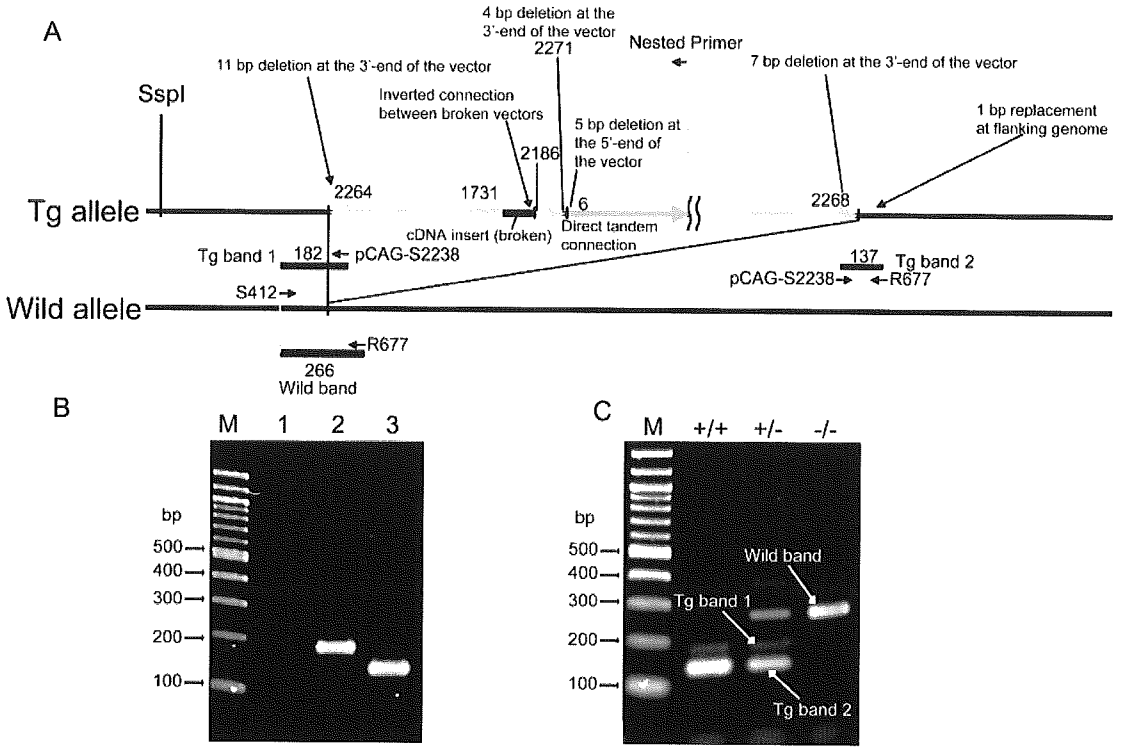

Fig. 2. Genomic configuration of GM1-sy#116, and the use of PCR to assess zygosity (A). The configuration of the transgene insert in the transgenic allele (Tg) and its corresponding wild-type allele (wild) are shown. One end of the insert was determined by genomic walking, and the other end by PCR with flanking primers. The directions of arrows over the inserts represent the 5'- to 3'-orientations of the vector constructs (arrowhead = 3'-end). Numbers along the inserts indicate the positions in pCAGGS. Approximately 10-bp deletions at each junction were detected, as shown in the figure. The positions of the three primers (S412, R677, and pCAG-S2238) used in a PCR experiment to determine zygosity, and the sizes of expected PCR products are also indicated. (B) Pre-evaluation of the PCR experiment. The primers were: lane 1, pCAG-S2238 only; lane 2, S412 and pCAG-S2238; lane 3, R677 and pCAG-S2238. M, 100-bp DNA ladder. (C) Determination of zygosity using PCR with the three primers, and genomic DNA from homozygous transgenic (+/+), hemizygous transgenic (+/–), and non-transgenic (–/–) mice. M, 100-bp DNA ladder.

polymerase (HotStarTaq; Qiagen, Hilden, Germany) in a Hybaid PCR Express Thermal Cycler (Thermo Hybaid, Ashford, Middlesex, UK). PCR products were separated by electrophoresis on a 2% agarose gel in Tris-acetate-EDTA buffer, and bands were detected by ethidium bromide staining and ultraviolet illumination (Figs. 1B, 2B and 2C).

Our method allowed the overall configuration of both ends of the transgene insert to be determined (Fig. 2A). One of the PCR bands (band f in Fig. 1B), which was approximately 1.5 kbp in length, contained about 500 bp of genome sequence flanking the transgene (Fig. 1C). A BLAST search of the sequence in the Ensembl database indicated that the transgene was inserted in the G2 region of chromosome 1 (Fig. 1D). The presence of an *Ssp*I restriction site in the genome sequence flanking the transgene was confirmed by the sequence around the transgene, which was retrieved from the database (data not shown). The full sequence of band f indicates the complicated insertion of constructs in the genome: one side of the genome faced the 3'-tail of a vector construct, and the construct was truncated at the middle of the inserted cDNA. Next to the truncated construct, direct repeats of the transgenes containing a short fragment of the 3'-tail of the construct were inversely concatenated and stretched at least to the position where the nested transgene-specific primer annealed. The structure of the other genome-transgene junction was revealed by PCR using three sets of flanking primers (Fig. 2B). No amplicons were produced by

PCR with pCAG-S2238 only (Fig. 2B-1), indicating the absence of tail-to-tail junction of transgenes as well as no formation of non-specific products by pCAG-S2238. The second set of primers (S412 and pCAG-S2238) confirmed one genome-transgene junction and showed a 182-bp band, as expected (Fig. 2B-2). The third set of primers (R677 and pCAG-S2238) showed a band of approximately 140 bp (Fig. 2B-3), which came from the other genome-transgene junctions. Direct sequencing confirmed that the band, which turned out to be 137 bp in length, was derived from the junction. Therefore, the 3'-tails of the transgenes were connected at both genome-transgene junctions. Although the full internal structure of the insert could not be identified by genomic walking, this is an example of irregular head-to-head type transgene-transgene junction, as described previously [12]. The zygosity was accurately determined using all three primers (Fig. 2C).

The mechanism of transgenesis is not fully understood, even though many kinds of transgenic animals have been produced (reviewed by e.g., [2]). Nevertheless, transgenesis seems to be accomplished in two steps: extrachromosomal concatenation of vector constructs, followed by integration into chromosomes [3]. Broad variation has been found at transgene-transgene and transgene-genome junctions in concatemers, such as deletions [7, 14], duplications [16], translocations of chromosomal DNA at the integration site [6, 13], and even insertions of sequences of unknown origin [16]. In our study, both types of junctions had approximately 10-base deletions, which may have been caused by so-called end-nibbling [14]. As Hamada *et al.* [7] discussed, the presence of nibbling at each junction suggests that linear concatemers were preferentially involved in the integration of the transgene into genomic DNA. Bishop [3] proposed a model in which concatemers are created by homologous recombination of circularly permuted linear molecules, which may explain the preferential formation of direct, rather than inverted, tandem repeats. In our case, however, it is more likely that concatemers of mixed orientation were formed by a simple random end-joining of DNA constructs, some of which had been fragmented before concatenation. While the fragmentation of DNA constructs can occur enzymatically inside zygote pronuclei, we suspect that the exposure to UV transillumination during gel-purification of our vector constructs was the most probable cause, because it has been shown that even a short period of transillumination induces serious DNA damage and profoundly reduces transformation frequencies [8]. Our results suggest that care should be taken to avoid unwanted fragmentation during the preparation of vector constructs.

Our results indicate that Bishop's model should be re-evaluated using a wide collection of transgenic patterns because of discrepancies with the fit of this model. In addition to events at transgene integration, attention should be paid to the possible involvement of the effect of transgene integration patterns on embryonic viability and modifications that occur after transgene integration, which are not accounted for by Bishop's model. If concatemer orientation affects embryonic viability, an embryo with direct (head-to-tail) tandem repeats of the transgene may be more viable than an embryo with inverted (head-to-head, tail-to-tail) tandem repeats. It is possible that inverted repeats that are integrated into the embryonic chromosome may be removed by palindrome deletion mechanisms [1]; if so, genomes of non-transgenic organisms may have transgene remnants (small fragments). Although difficult ($\leq$ 20% of transformed embryos reach birth [4]), further analysis of transgenic organisms would test the validity of this hypothesis.

Our results demonstrate the usefulness of the genomic walking technique to determine both the structure of transgenes and their flanking sequences. Together with gene expression assays, this technique should provide a powerful tool for revealing relationships between insertion pattern and expression efficiency of transgenes.

References

1. Akgun, E., Zahn, J., Baumes, S., Brown, G., Liang, F., Romanienko, P.J., Lewis, S., and Jasin, M. 1997. *Mol. Cell. Biol.* 17: 5559–5570.
2. Auerbach, A.B. 2004. *Acta Biochim. Pol.* 51: 9–31.
3. Bishop, J.O. 1996. *Reprod. Nutr. Dev.* 36: 607–618.
4. Brinster, R.L., Chen, H.Y., Trumbauer, M.E., Yagle, M.K., and Palmiter, R.D. 1985. *Proc. Natl. Acad. Sci. USA* 82: 4438–4442.
5. Daniotti, J.L., Martina, J.A., Zurita, A.R., and Maccioni, H.J. 1999. *J. Neurosci. Res.* 58: 318–327.
6. Gordon, J.W. and Ruddle, F.H. 1985. *Gene* 33: 121–136.
7. Hamada, T., Sasaki, H., Seki, R., and Sakaki, Y. 1993. *Gene* 128: 197–202.
8. Hartman, P.S. 1991. *Biotechniques* 11: 747–748.
9. Hubbard, T., Barker, D., Birney, E., Cameron, G., Chen,

Y., Clark, L., Cox, T., Cuff, J., Curwen, V., Down, T., Durbin, R., Eyras, E., Gilbert, J., Hammond, M., Huminiecki, L., Kasprzyk, A., Lehvaslaiho, H., Lijnzaad, P., Melsopp, C., Mongin, E., Pettett, R., Pocock, M., Potter, S., Rust, A., Schmidt, E., Searle, S., Slater, G., Smith, J., Spooner, W., Stabenau, A., Stalker, J., Stupka, E., Ureta-Vidal, A., Vastrik, I., and Clamp, M. 2002. *Nucleic Acids Res.* 30: 38–41.

10. Nagy, A., Gertsenstein, M., Vintersten, K., and Behringer, R. 2003. pp. 507–540. *In*: *Manipulating the Mouse Embryo*, Cold Spring Harbor Laboratory Press, New York.
11. Niwa, H., Yamamura, K., and Miyazaki, J. 1991. *Gene* 108: 193–199.
12. Noguchi, A., Takekawa, N., Einarsdottir, T., Koura, M., Noguchi, Y., Takano, K., Yamamoto, Y., Matsuda, J., and Suzuki, O. 2004. *Exp. Anim.* 53: 103–111.
13. Overbeek, P.A., Lai, S.P., Van Quill, K.R., and Westphal, H. 1986. *Science* 231: 1574–1577.
14. Rohan, R.M., King, D., and Frels, W.I. 1990. *Nucleic Acids Res.* 18: 6089–6095.
15. Rozen, S. and Skaletsky, H.J., *Primer3. Code available at http://www-genome.wi.mit.edu/genome_software/other/primer3.html.* 1998.
16. Wilkie, T.M. and Palmiter, R.D. 1987. *Mol. Cell. Biol.* 7: 1646–1655.

J Inherit Metab Dis, in press, 2006

β-Galactosidase Deficiency: An Approach to Chaperone Therapy

Yoshiyuki Suzuki

International University of Health and Welfare, Otawara, Japan

Correspondence Address:

Yoshiyuki Suzuki, M.D.

Clinical Research Center, International University of Health and Welfare

2600-1 Kita-Kanemaru, Otawara 324-8501, Japan

Tel / Fax: 81-287-24-3229

Email: SuzukiY@iuhw.ac.jp

Key Words

Chaperone therapy, G_{M1}-gangliosidosis, β-Galactosidase, N-Octyl-4-epi-β-valienamine, Disease model mouse

Summary

We propose a new molecular therapeutic approach to lysosomal diseases with severe neurological manifestations. Some low molecular compounds, acting as competitive inhibitors of a lysosomal enzyme *in vitro*, were found to stabilize and restore catalytic activities of the enzyme molecule as a molecular chaperone. We started this trial first to Fabry disease (generalized vasculopathy) using galactose and 1-deoxygalactonojirimycin, and then to β-galactosidase deficiency disorders (β-galactosidosis) with generalized neurosomatic and/or systemic skeletal manifestations (G_{M1}-gangliosidosis and Morquio B disease), using a newly developed chemical compound N-octyl-4-epi-β-valienamine (NOEV). Administration of this chaperone compound resulted in elevation of intracellular enzyme activity in cultured fibroblasts from patients and genetically engineered model mice. In addition, substrate storage was improved after NOEV had been transported in the brain tissue via the blood-brain barrier. We hope this new approach (chemical chaperone therapy) will be useful for certain patients with β-galactosidosis and potentially other lysosomal storage diseases with central nervous system involvement.

Introduction

G_{M1}-gangliosidosis (OMIM 230500) is a neurogenetic disease caused by mutations of the gene GLB1 (3p21.33) that codes for lysosomal β-galactosidase (EC 3.2.1.23) with clinical onset at various ages (Suzuki et al, 2001). They are classified as infantile, juvenile, and adult forms. In addition another rare systemic bone disease, Morquio B disease, is known also to be caused by other different mutations of the same gene, resulting in β-galactosidase deficiency. Glycoconjugates with terminal β-galactose residues accumulate in tissues and body fluids from patients with these clinical phenotypes. Ganglioside G_{M1} and its asialo derivative G_{A1} accumulate in the G_{M1}-gangliosidosis brain. High amounts of oligosaccharides derived from keratan sulfate or glycoproteins are detected in visceral organs and urine from G_{M1}-gangliosidosis and Morquio B disease patients.

At present only symptomatic therapy is available for human β-galactosidosis patients. Allogeneic bone marrow transplantation did not modify subsequent clinical course or cerebral enzyme activity in a Portuguese water dog affected with G_{M1}-gangliosidosis (O'Brien et al, 1990). Amniotic tissue transplantation was not effective in a patient with Morquio B disease (Tylki Szymanska et al, 1985). Enzyme replacement therapy conducted for Gaucher disease and other lysosomal storage diseases is not available at present for β-galactosidosis. An experiment to inhibit G_{M1} synthesis resulted in reduction of the G_{M1} content in the mouse brain, but not G_{A1} (Kasperzyk et al, 2004; 2005). More evaluation is necessary for the therapeutic trial of this type.

We tried to develop a new therapeutic approach to lysosomal storage diseases, particularly with the central nervous involvement. A molecular analysis revealed that some mutant proteins expressed in the culture cells from Fabry patients do not exhibit the catalytic activity because of molecular instability of the molecule (Okumiya et al, 1995a). Subsequently the unstable protein was found to have a defect in molecular folding and rapid degradation after biosynthesis (Ishii et al, 1996). Zhang *et al.* (2000) reported the same result

in a study of the mutant enzyme in an infantile G_{M1}-gangliosidosis patient. The R148S β-galactosidase mutation resulted in a major conformational change of the protein molecule with normal catalytic activity, and failed to reach the lysosome.

Simultaneously, trials to stabilize the mutant protein revealed that galactose in the culture medium was able to induce a high expression of the mutant α-galactosidase A gene in cultured lymphoblasts in both classical and atypical (cardiac) form of Fabry disease (Okumiya et al, 1995b). This result prompted us to search for more potent inducers of mutant gene expression among commercially available chemical compounds structurally similar to galactose. 1-Deoxygalactonojirimycin (DGJ) was found to be the best candidate for a possible new molecular therapy of Fabry disease in cultured lymphoblasts and transgenic mice (Fan et al, 1999).

Concept of chaperone therapy

There are three possible types of mutant gene expression in somatic cells.

1. No biosynthesis of the mutant protein.
2. Extremely low or completely deficient activity of the expressed mutant protein.
3. Expression of unstable mutant protein with normal or near-normal catalytic activity.

We tested these possibilities in Fabry disease, and found a surprisingly high percentage of the third possibility in Fabry disease and β-galactosidosis, although the rate of effectiveness depends on the definition of therapeutic effect in culture cell experiments (Iwasaki et al, unpublished data). These mutant proteins are unstable at neutral pH in the endoplasmic reticulum/Golgi apparatus, and are rapidly degraded without appropriate molecular folding (Okumiya et al, 1995a; Ishii et al, 1996).

After galactose we found a commercially available compound DGJ for induction of enhanced mutant gene expression and enzyme activity of α-galactosidase A (Fabry disease; Fan et al, 1999). Next, new chemically synthesized compound were tried for this new

approach: N-octyl-4-epi-β-valienamine (NOEV) for β-galactosidase (G_{M1}-gangliosidosis and Morquio B disease; Matsuda et al, 2003) and N-octyl-β-valienamine (NOV) for β-glucosidase (Gaucher disease; Lin et al, 2004) (Figure 1).

Exogenous compounds that inhibit enzyme activity *in vitro* bind to the mutant enzyme intracellularly around endoplasmic reticulum/Golgi apparatus, resulting in formation at neutral pH of a complex consisting of the mutant protein and chaperone compound. The catalytically active mutant gene is now stabilized, and the protein-chaperone complex is safely transported to the lysosome. The complex dissociates under the acidic condition in the lysosome, and the mutant enzyme remains stabilized and its catalytic function is expressed (Figure 2).

This strategy depends on the biological activity of the chaperone compound available for the study. In a previous study, we had to add a high dose of galactose (up to 200 mM) in the culture medium of Fabry cells (Okumiya et al, 1995b). This is obviously unnatural and deleterious to the function of somatic cells for a long-term treatment, although a short-term human experiment demonstrated a positive therapeutic effect after high-dose intravenous galactose in a Fabry patient (Frustaci et al, 2001).

NOEV was more efficient than DGJ for expression of β-galactosidase activity in G_{M1}-gangliosidosis as compared to α-galactosidase A activity in Fabry disease (Tominaga et al, 2001; Matsuda et al, 2003). Our calculation indicates that at least 10% normal enzyme activity is necessary for washout of the storage substrate in lysosomal diseases. The age of onset in patients expressing the enzyme activity above this level will be theoretically beyond the human life span (unpublished data).

Determination of intracellular chaperone concentration is technically not possible at present. We anticipate NOEV concentrations in human cells and animal tissues are much lower than IC_{50} of NOEV in vitro. In fact, the NOEV concentration in the tissue culture medium was approximately the IC_{50} in our cell culture experiments (Matsuda et al, 2003).

NOV and NOEV: Chemical synthesis and characterization

Fortunately we found a commercially available compound DGJ for possible chaperone therapy of Fabry disease (Fan et al, 1999). However, an extensive search for other galactose derivatives and analogous compounds did not reveal any material significantly active for β-linked galactose substrates. I happened to come across an inhibitor originally synthesized for chemical analysis of enzyme reaction catalyzed by glucocerebrosidase (β-glucosidase): NOV (Ogawa et al, 1994; 1995; 1998). Gaucher disease is caused by deficiency of this enzyme. Then, we tried to develop chemical compounds related to this glucose derivative.

First, NOV was synthesized by chemical modification of the original glucocerebrosidase inhibitor, followed by replacing the ceramide moiety with simple aliphatic chains (Ogawa et al, 1996, 1998). Subsequently, NOEV was synthesized by multi-step epimerization of NOV at C-4 (Ogawa et al, 2002; 2004). Both NOV and NOEV (Figure 2) were tested simultaneously, but characterization and evaluation of NOEV moved faster than NOV simply because we had more experience in β-galactosidase and collected more clinical samples from patients with β-galactosidase deficiency.

NOEV is a potent inhibitor of lysosomal β-galactosidase *in vitro*. Addition of NOEV in the culture medium restored mutant enzyme activity in cultured human or murine fibroblasts at low intracellular concentrations, resulting in a marked decrease of intracellular substrate storage (see below). Its structure was assigned by a combination of COSY, TOCSY and HSQC NMR spectroscopy (Matsuda et al, 2003). NOEV is a stable compound at room temperature, and a strong inhibitor of human β-galactosidase *in vitro*. It is freely soluble in methanol or dimethylsulfoxide, and soluble in water up to 3-5 mM at room temperature. The molecular weight is 287.40. The IC_{50} is 0.2 μM toward human β-galactosidase.

NOEV effect on in cultured human and mouse fibroblasts expressing mutant human genes

In human fibroblast experiments, the cells derived from juvenile and infantile G_{M1}-gangliosidosis patients expressed an increase of β-galactosidase activity after NOEV treatment (Iwasaki et al, unpublished data). Under the conditions of our study, we found two different response types among the cells for analysis. Some cells responded to NOEV maximally at 0.2 μM, such as R457Q, and the others at 2 μM, such as R201C and R201H. This result indicates that the molecular interaction between the chaperone compound and mutant protein is mutation-specific.

The mouse fibroblasts expressing mutant human β-galactosidase showed essentially the same results (Matsuda et al, 2003). However, the degree of enhancement was different in some mutations between the human and mouse cells. An increase of 5-10-fold increase was observed for the R427Q mutation at 0.2 μM of NOEV in the culture medium. A higher concentration (2 μM) was necessary for the R201C or R201H mutation to the same degree (Iwasaki et al, unpublished data). About one-third of the cells from patients with G_{M1}-gangliosidosis responded to this treatment; almost all patients with juvenile G_{M1}-gangliosidosis, and some of the patients with infantile G_{M1}-gangliosidosis responded significantly. Almost the same or more restorative effect was achieved with NOEV at 50-fold lower concentration than that with 1-deoxygalactonojirimycin or N-butyl-deoxygalactonojirimycin (Tominaga et al, 2001).

After adding the mixture of gangliosides to the culture medium, intracellular G_{M1} increased remarkably in R201C cells. but only slightly in the cells expressing the normal human gene. Incubation with NOEV significantly reduced G_{M1} storage in the cells expressing the mutation R201C causing juvenile G_{M1}-gangliosidosis (Matsuda et al, 2003).

Chaperone therapy on genetically engineered G_{M1}-gangliosidosis model mice